Journal of Infectious Diseases Advance Access published October 20, 2015

Middle East Respiratory Syndrome Coronavirus Causes Multiple Organ Damage and Lethal Disease in Mice Transgenic for Human Dipeptidyl Peptidase 4

Kun Li[1], Christine Wohlford-Lenane[1], Stanley Perlman[1,2,5], Jincun Zhao[2], Alexander K. Jewell[1], Leah R. Reznikov[3], Katherine N. Gibson-Corley[4], David K. Meyerholz[4], Paul B. McCray, Jr.[1,2,*]

[1]Department of Pediatrics, University of Iowa, Iowa City, IA 52242

[2]Department of Microbiology, University of Iowa, Iowa City, IA 52242

[3]Department of Internal Medicine, University of Iowa, Iowa City, IA 52242

[4]Department of Pathology[4], University of Iowa, Iowa City, IA 52242

[5]Department of Interdisciplinary Program in Immunology, University of Iowa, Iowa City, IA 52242

[*]Corresponding author: Paul McCray, Department of Pediatrics, 6320 PBDB, University of Iowa, Iowa City, IA 52242, tel. 319-335-6844, Fax. 319-335-6925, Email: paul-mccray@uiowa.edu

Notes

Acknowledgements

We thank Sateesh Krishnamurthy, Jennifer Bartlett, and Patrick Sinn for careful review of the manuscript. We thank Jim Hu for providing the K18 plasmid construct.

Financial Support

This work is supported by the National Institutes of Health PO1 AI060699. We also acknowledge the support of the Cell Morphology Core and Pathology Core, partially supported by the Center for Gene Therapy for Cystic Fibrosis (National Institutes of Health P30 DK-54759) and the Cystic Fibrosis Foundation, and of the Transgenic Mouse Facility supported in part by the College of Medicine and by the Center for Gene Therapy for Cystic Fibrosis. P.B.M. is supported by the Roy J. Carver Charitable Trust.

Potential Conflict of Interest

The authors declare that they have no competing financial interests.

Corresponding author

Paul McCray, Department of Pediatrics, 6320 PBDB, University of Iowa, Iowa City, IA 52242, tel. 319-335-6844, Fax. 319-335-6925, Email: paul-mccray@uiowa.edu

ABSTRACT

Middle East respiratory syndrome (MERS)-coronavirus (MERS-CoV) causes life threatening disease. Dipeptidyl peptidase 4 (DPP4) is the receptor for cell binding and entry. There is a need for small animal models of MERS, but mice are not susceptible to MERS because murine dpp4 does not serve as a receptor. We developed transgenic mice expressing human DPP4 (hDPP4) under the control of the surfactant protein C promoter or cytokeratin 18 promoter that are susceptible to infection with MERS-CoV. Notably, mice expressing hDPP4 with the cytokeratin 18 promoter developed progressive, uniformly fatal disease following intranasal inoculation. High virus titers were present in lung and brain tissues at 2 and 6 d.p.i., respectively. MERS-CoV infected lungs revealed mononuclear cell infiltration, alveolar edema, and microvascular thrombosis, with airways generally unaffected. Brain disease was observed with the greatest involvement noted in the thalamus and brainstem. Animals immunized with a vaccine candidate were uniformly protected from lethal infection. These new mouse models of MERS-CoV should be useful for investigation of early disease mechanisms and therapeutic interventions.

BACKGROUND

Middle East Respiratory Syndrome (MERS) first emerged on the Saudi Arabian peninsula in 2012. A new coronavirus, MERS-CoV, was identified as the causative agent [1] and dipeptidyl peptidase 4 (DPP4, CD26) was identified as its receptor [2]. The disease spectrum ranges from asymptomatic cases to the acute respiratory distress syndrome, circulatory collapse, multiorgan failure, and death [3]. As of 5 October 2015 the WHO has been notified of 1,589 laboratory-confirmed cases of MERS-CoV infection in more than two dozen countries, resulting in at least 567 related deaths. The greatest mortality occurs in the elderly and those with comorbidities [4-7].

Epidemiologic studies indicate that MERS-CoV can spread to humans from infected dromedary camels [8]. A closely related virus is resident in wild bats, suggesting that they serve as natural reservoirs for MERS-like viruses [9]. Although human to human or zoonotic spread of MERS has not reached epidemic or pandemic levels, its potential to spread between persons was demonstrated in healthcare settings in the Middle East [10] and by the recent outbreak in South Korea caused by a single infected individual [11].

MERS-CoV can infect rabbits and camels, and some species of non-human primates (rhesus macaques and common marmosets, reviewed in [12]). Marmosets develop a severe progressive lung disease although this has recently been questioned [45]. The other animals develop a more mild, self-limited respiratory illness [13]. Because large animal and primate studies are resource intensive, a small animal model is desirable. The MERS-CoV spike (S) glycoprotein does not bind the murine dpp4 protein efficiently, therefore preventing infection [14, 15]. We reported

that mice sensitized to MERS-CoV by adenoviral transduction of *hDPP4* to pulmonary epithelia confers productive virus replication, allowing rapid screening of phenotypes in genetically modified mouse strains [16].

A transgenic mouse model would help investigate MERS pathogenesis and aid development of vaccine and antiviral therapies, in part because reagents to study the immune response are widely available. Recently, Agrawal reported mice expressing a *hDPP4* transgene with the ubiquitous CAGGS promoter (CMV immediate-early enhancer and chicken β-actin promoter) [17]. When exposed to MERS-CoV (10^6 $TCID_{50}$, intranasally) these mice exhibited progressive weight loss and died with evidence of high virus titers and inflammatory responses in lung and brain tissues. They detected virus antigen in the heart, spleen, and intestine, indicating spread beyond the lungs and brain. To develop new MERS models, we generated mice expressing hDPP4 in epithelial cells using two different cell type specific promoters. We show that transgenic expression of hDPP4 in epithelia facilitates MERS-CoV replication in lung tissue. Depending on the promoter selected, the disease outcome ranged from mild and self-limited to lethal with lung and brain tissue involvement.

METHODS

Generation of human DPP4 transgenic mice. All studies were approved by the Animal Care and Use Committee of the University of Iowa. We used two different promoters (cytokeratin 18 or surfactant protein C) to direct hDPP4 expression in epithelia (Figure 1A; Supplemental Figure 1A). A FLAG epitope tagged hDPP4 cDNA (Origene) was cloned into the pK18mTElacZ-K18i6x7pA vector to create pK18-*hDPP4* [18-20]. The human SPC promoter, a gift from Dr.

Teodora Georgieva (BIO5 Institute, Tucson, AZ), was used to generate the pSPC-*hDPP4* vector. Purified DNA fragments from the pK18-*hDPP4* and pSPC-*hDPP4* vectors were injected into pronuclei of fertilized B6SJL (C57BL/6J X SJL/J) mouse eggs to generate transgenic embryos. Mice transgenic for *hDPP4* expression were detected by PCR using the following primers: forward primer: CCA AAG ACT GTA CGG GTT CC; reverse: CCA AAG CTG AAT TGT CTT CCA G**.**

Infection of transgenic mice with MERS-CoV. The MERS-CoV (EMC2012 strain, passage 8) was provided by Drs. Bart Haagmans and Ron Fouchier (Erasmus Medical Center). Virus was propagated and titered by plaque assay on Vero-81 cells. Mice expressing hDPP4 were anesthetized with ketamine/xylazine and infected intranasally with MERS-CoV in 50 µl DMEM. Mice were examined daily and temperatures and weights recorded. Non-transgenic littermates served as controls. MERS-CoV work was conducted in a Biosafety Level 3 (BSL3) Laboratory.

Virus Titers. Tissues were removed aseptically, disassociated with a manual homogenizer in 1X PBS, briefly centrifuged, and supernatants removed. Samples were titered on Vero-81 cells as reported [16].

DPP4 protein abundance. DPP4 protein abundance was measured by ELISA (human DPP4 DuoSet, catalog #DY1180, R&D Systems, Minneapolis, MN) following the manufacturer's protocol.

Extraction of Total RNA and Quantitative RT-PCR. See Supplemental Materials

Histology and immunohistochemistry. See Supplemental Materials

MERS-CoV infection of human cell lines and primary porcine astrocytes. The human neuroblastoma cell line SK-N-SH was grown in RPMI 1640 with 10% FBS. The glioma cell line U138MG and murine astrocytoma cell line DBT cells were cultured in DMEM with 10% FBS. Primary porcine glial cells were cultured as previously described [21]. Dissociated cells were allowed to attach to collagen-coated plates and cultured for 2-3 weeks. Cells were infected with MERS-CoV at MOI of 1. At time 0 and two days after infection, supernatants were harvested for titers and cells processed for immunostaining.

Inhibition of MERS-CoV infection by passive and active immunization. Venezuelan equine encephalitis replicon particles (VRPs) expressing the MERS-CoV spike (S) glycoprotein or GFP were constructed as previously described [16]. K18-*hDPP4* transgenic mice were immunized in the foot pad with 1×10^5 infectious units (IU) of VRP-S or VRP-GFP in 20 µl of PBS and boosted with the same doses 4 weeks later. Two weeks after the second immunization, mice received 1×10^5 PFU of MERS-CoV. For passive immunization, non-transgenic mice received 1×10^5 IU of VRP-S or VRP-GFP and then were boosted with the same dose 4 weeks later. Two weeks later serum was harvested and 300 µl of serum transferred into K18-*hDPP4* mice intraperitoneally 1 day before MERS-CoV infection.

Statistical analysis. Student's t-test or ANOVA with Dunn's multiple comparison test were used to analyze differences in mean values between groups unless otherwise specified. Results are expressed as mean +/- standard error or standard deviation, as indicated. P values ≤0.05 were considered significant.

RESULTS

Characterization of hDPP4 transgenic mice. DPP4 is broadly expressed in human tissues and cells (reviewed in [22]). In primary cell culture and organ culture models, MERS-CoV predominantly infects non-ciliated epithelial cell types of the respiratory tract [2, 23]. To direct MERS-CoV receptor expression to pulmonary epithelia, we used the surfactant protein C (SPC) promoter (Supplemental Figure 1A) or the cytokeratin 18 (K18) promoter (Figure 1A) as described in Methods. The SPC promoter drives expression in bronchiolar and alveolar epithelia [24]. In contrast, the *K18* promoter confers transgene expression in airway and alveolar epithelial cells, as well as epithelia of the liver, kidney and gastrointestinal tract, and some cells of the nervous system [18]. We generated 8 SPC-*hDPP4* founder lines and 4 K18-*hDPP4* founder lines.

We first screened F2 mice from each founder line for evidence of a pulmonary infection following intranasal (i.n.) inoculation with 1 x 10^5 PFU of MERS-CoV. We identified three SPC-*hDPP4* lines (Supplemental Figure 1B) and two K18-*hDPP4* lines (Figure 1B) with productive MERS-CoV infections based on titers 3 days post infection (d.p.i.). The titers achieved in the K18-*hDPP4* lines exceeded those of the SPC-*hDPP4* lines. We selected founder line 3 from both the SPC-*hDPP4* and K18-*hDPP4* lines for additional studies, as these showed

the highest virus titers 3 d.p.i. Intranasal infection of transgenic mice and their non-transgenic littermates from SPC-*hDPP4* line 3 with MERS-CoV caused no mortality or changes in body temperature, but mice failed to gain weight compared to non-transgenic littermates (Supplemental Figures 1C-F). Virus was cleared by 14 d.p.i.

MERS-CoV-infected K18-*hDPP4* mice develop lethal disease. We detected DPP4 protein expression in brain, heart, lung, kidney, spleen, intestine, and liver of K18-*hDPP4* mice (Figure 1C). In contrast to the SPC-*hDPP4* transgenic mice, K18-*hDPP4* mice inoculated intranasally with MERS-CoV uniformly exhibited weight loss and hypothermia, and died at 6-7 d.p.i. (Figures 2A-C). MERS-CoV titers were highest in lung tissue 2 d.p.i. (6×10^7 PFU/g tissue) and then declined at 4 and 6 d.p.i. In contrast, virus titers in brain were undetectable at 2 d.p.i. and then increased to 10^5 and 10^8 PFU/gram tissue at 4 and 6 d.p.i., respectively (Figure 2D). Although the K18 promoter is active in the epithelia of multiple organs, no virus was titered from the kidney (Figure 2D). We quantified virus RNA distribution in tissues and blood by PCR at 2 and 4 d.p.i. (Figure 2E). Virus RNA was abundant in lung at 2 and 4 d.p.i. RNA was detected in brain tissue at 4 d.p.i. Lower levels of viral RNA were also detected in spleen 2 d.p.i. and kidney and heart 4 d.p.i.

We also asked whether MERS-CoV infected mice could spread the virus to other animals. MERS-CoV was not transmitted from infected K18-*hDPP4* mice (n=2) to uninfected K18-*hDPP4* mice (n = 3) housed in the same cages (data not shown). No virus RNA was detected in the brain, lung, or blood of these healthy co-housed mice (data not shown). This was not surprising, however, since mice do not cough or sneeze.

Histopathology of K18-*hDPP4* lung tissue infected with MERS-CoV. MERS-CoV infection in lung was evaluated and scored at 2, 4, and 6 d.p.i. (Table 1). MERS-CoV infection produced patchy consolidation (Figure 3A) variably composed of cellular inflammation, vascular congestion, and atelectasis. The airways were generally intact with only scattered, uncommon sloughed cells (Figure 3B). In some lungs, lymphatic vessels were filled with degenerative cells and cellular debris (Figure 3C). Thrombi (Figure 3D) were also observed with nearby vascular congestion, and lesser hemorrhage and necrosis. Alveolar edema was detected in some lung fields (Figure 3E). We investigated virus antigen expression in the lungs at 2, 4, 6 d.p.i. (Supplemental Figure 2). MERS-CoV N protein was most abundant in the lung parenchyma in alveolar type I and II cells, and in macrophages.

Nervous system disease in MERS-CoV-infected K18-*hDPP4* mice. MERS-CoV was detected at high levels in infected K18-*hDPP4* mice. Transgenic hDPP4 expression in brain was corroborated by ELISA (Figure 1C). We evaluated pathologic changes in the brains of MERS-CoV infected mice at 2, 4, and 6 d.p.i. (Table 2). Compared to controls (Figure 4A), MERS-CoV infected mice exhibited perivascular cuffing (Figures 4B, E), cellular degeneration and debris (Figures 4C, D) that was absent at day 2 with progressive changes from days 4 to 6 (Table 2). Degenerating and dying neurons sometimes had basophilic cytoplasmic inclusions that were quite prominent (Figures 4C, F) and immunostained for viral antigen (Figure 4F). MERS-CoV induced neuronal lesions were most severe in the thalamus and brainstem (Table 2). More detailed virus antigen staining in brain tissue at 2, 4, 6 d.p.i. is shown in Supplemental Figure 3. N protein staining was rare at 2 and 4 d.p.i. and principally seen in solitary neurons. In contrast, by 6 d.p.i. many neurons were infected. Virus antigen at 6 d.p.i. was preferentially located in

midbrain, thalamus, deep cerebral cortex, and CA2 region of hippocampus, but was uncommon in the cerebellum.

Collectively, these results show that both the lungs and brain developed pathological changes after MERS-COV infection. To differentiate the importance of brain versus lung infection, we used low inoculum doses, in order to optimize the likelihood that only the brain or the lung would be infected. We used intranasal inocula of 1,000, 100, and 10 PFU/animal. Compared to mice receiving a larger inoculum, the onset of weight loss was delayed from 3-4 d.p.i. to 9-10 d.p.i. (Figures 4G-I). Despite this delayed onset of disease signs, 4/5 mice succumbed with the 1,000 PFU inoculum, 4/5 mice died with a 100 PFU inoculum, and 3/5 mice succumbed following a 10 PFU inoculum. In a second experiment, MERS-CoV was detected in brain tissue of 3/7 mice infected with 10 PFU (~4 x 10^6 PFU/g tissue) at 9 d.p.i. No virus was titered from lung tissue (Figure 4I). Thus mortality correlated with brain infection, suggesting that infection of this organ was most important for the high mortality observed in K18-*hDPP4* mice.

MERS-CoV infection of cells from the nervous system. The clinical course of MERS in severely ill patients sometimes includes neurological manifestations [4, 25], suggesting that MERS-CoV may infect the human central nervous system (CNS). Of note, DPP4 is expressed in vascular endothelia and other brain cell types [22, 26-33]. To determine whether MERS-CoV could infect and complete its replication cycle in CNS-derived cells, we infected CNS-derived human cell lines or primary astrocytes derived from newborn pig brain tissue. Pig cells were previously shown to be permissive to MERS-CoV infection [2]. Human cell lines (U-138 MG, SK-N-SH) and primary porcine astrocytes all expressed DPP4 protein (data not shown). SK-N-

SH cells, porcine astrocytes, and control Vero-81 cells supported virus replication (Figure 4J) and this result was confirmed by immunostaining for MERS-CoV antigen (Supplemental Figure 3). No human autopsy samples are available to directly assess virus replication in the brain, but these results support the notion that neurological disease is directly virus-induced.

Induction of proinflammatory cytokines and chemokines in MERS-CoV-infected K18-*hDPP4* mice. Based on studies of cells infected *in vitro* [34-37], dysregulated cytokine and chemokine production is postulated to contribute to disease severity. We profiled the expression of several cytokine, chemokine, and antiviral gene products in lung and brain tissues 2, 4, and 6 d.p.i. using qRT-PCR. As shown in Supplemental Figure 4, we observed an overall trend that these host defense gene products were first induced in the lung, followed by a later increase in signal in the brain. In the lung there were significant increases in type I, II, and III interferons by 2 d.p.i. The induction of interferon lambda in lung was especially remarkable. Upregulation of all classes of interferons occurred later in brain tissue and did not reach the same levels as lung with the exception of interferon gamma. Several other gene products were increased early in the lung including ISG15, IL-6, IL-12p40, IL-15, CCL2, CXCL9, and CXCL10. Peak expression of RIG-I, MDA5, PKR, MYD88, TNF-α, IL-1β, CCL2, CCL5, and CXCL10 was greater in the brain than lung at the later time points.

Kidneys from MERS-CoV infected mice. Renal failure is commonly seen in MERS patients but it is not known whether the kidney is infected by the virus. MERS-CoV infected mice had scattered to patchy evidence of tubular injury including tubular dilation, cell sloughing/debris, and cellular necrosis (Supplemental Figure 5). These changes were principally seen late in the

course of infection (6 d.p.i., 9/9 cases) and otherwise only seen rarely / focally at 4 d.p.i. (3/3 cases) and not detected at 2 d.p.i. (0/3 cases). Consistent with published results [17], no virus was detected in the kidneys of MERS-CoV infected animals at 2, 4, or 6 d.p.i. These pathologic changes are most consistent with shock or hypoxia.

Active or passive immunization of K18-*hDPP4* mice prevents clinical disease. To determine whether K18-*hDPP4* mice will be useful for evaluating anti-MERS-CoV vaccines or therapies, we vaccinated K18-*hDPP4* mice with VRPs expressing the MERS-CoV surface spike (S) glycoprotein (VRP-S) or VRP-GFP prior to MERS-CoV infection. Following a primary and secondary immunization, mice were challenged with 1 x 10^5 PFU of MERS-CoV intranasally. As shown in Figures 5A, B, immunized mice were completely protected against lethal infection. Mice immunized with VRP-S showed 100% survival and no weight loss over the course of the 14 day experiment.

Next, animals were pre-treated with serum from mice immunized with VRP-S or VRP-GFP. Intraperitoneal administration of serum from mice immunized with VRP-S one day prior to MERS-CoV infection completely prevented the lethal disease manifestations in K18-*hDPP4* mice including weight loss and clinical disease (Figures 5C, D). Control anti-GFP sera treated mice all died. We also assessed tissue titers in MERS-CoV infected mice following passive immunization at 2, 4, and 6 d.p.i. We observed an accelerated reduction in lung tissue titers in immunized mice, with no virus titered after 4 d.p.i. (Figures 5E). Passive immunization completely prevented spread of infection to the brain (Figure 5F).

DISCUSSION

The recent outbreak in South Korea demonstrates that MERS-CoV continues to pose significant risks to human health [11]. Here we report new mouse models of MERS-CoV infection. Because the restriction in infecting mouse cells with MERS-CoV is at the level of the receptor [14, 15], we generated mice expressing human DPP4 under control of the surfactant protein C or cytokeratin 18 promoters. When challenged with MERS-CoV, a fatal disease course ensued in K18-*hDPP4* mice, with inflammatory disease involving lung and brain tissues. In this setting of severe disease, immunization with VRPs expressing the MERS-CoV spike glycoprotein conferred protective immunity. SPC-*hDPP4* mice exhibited a milder disease phenotype. These transgenic mice provide new models for investigation of MERS-CoV infection and the evaluation of therapeutic interventions.

Several animal species have been tested for their susceptibility to MERS-CoV respiratory infection and disease. Mice [38], Syrian hamsters [39], and ferrets [40] do not support MERS-CoV replication. In contrast, rhesus macaques [41, 42], marmosets [13], rabbits [43], and camels [44] all allow the virus to complete its replication cycle. While marmosets develop significant lung pathology with associated mortality when given a large inoculum [13], others report minimal disease in marmosets [45]. The phenotypes in other mammals studied are mild and do not recapitulate a severe MERS-like disease.

Zhao and coworkers reported the first mouse model of MERS infection [16]. They sensitized mice to MERS-CoV infection by delivering adenovirus vectors expressing hDPP4 to the lungs of mice. However, only the lung expressed hDPP4 so virus replication in other organs could not be

evaluated. Agrawal expressed *hDPP4* behind a universally expressed promoter [17]. Here we expanded the available mouse models by stably expressing *hDPP4* with the SPC and K18 promoters. Both of these promoters exhibit more restricted expression compared to the CAGGs promoter used by Agrawal et al [17]. The disease phenotype of the K18-*hDPP4* mice shares many features with the results reported by Agrawal [17], including fatal disease with lung and brain involvement. In contrast, the SPC-*hDPP4* line demonstrated lower lung tissue viral loads than Ad-*hDPP4* sensitized mice [16] without spread to other organs or associated mortality. This suggests that with infection restricted to the lung, mouse innate immunity may successfully overcome virulence factors expressed by MERS-CoV and prevent a lethal outcome. A mouse adapted MERS-CoV strain may help overcome this limitation.

The K18-*hDPP4* transgenic mice developed several disease features of interest. Analysis of the lungs at 2, 4, and 6 d.p.i. revealed ongoing virus replication and significant parenchymal involvement. In addition, the airways exhibited rare sloughed cells and cell debris was observed within lymphatic vessels. These changes were associated with increases in several innate immune molecules and cytokines including type I, II, and III interferons, ISG15, IL-6, IL-12p40, IL-15, CCL2, CXCL9, and CXCL10. Interestingly, interferon lambda, the predominant mucosal interferon in the lung [46], was markedly induced in the lung of MERS-CoV infected mice. These lung disease features provide several quantitative endpoints for evaluation of efficacy of antiviral therapies.

We previously used the K18 promoter to generate mice transgenic for human ACE2 as a model for SARS-CoV infection [20]. Following infection with the Urbani strain of SARS-CoV, K18-

hACE2 mice developed a lethal disease featuring both lung and brain involvement. SARS-CoV spread from the olfactory bulb to primary, secondary, and more distal connections very rapidly, resulting in lethality. In the present study, the temporal course of brain tissue infection also suggested retrograde virus spread from olfactory neurons. While susceptibility to brain infection sets a high bar for evaluating new therapies for MERS-CoV infection, we demonstrated the utility of the model for vaccine testing. We acknowledge that high titer replication and death by CNS disease in K18-*hDPP4* transgenic mice may complicate the study of some vaccines and other therapeutic interventions, especially for drugs that do not cross the blood-brain barrier.

The K18-*hDPP4* mice developed lethal disease with encephalitis contributing to their demise. Is the brain infection in a mouse model of MERS relevant to the disease in humans? We note that DPP4 is expressed in the brains of humans and other mammals [22, 26-33]. We found that MERS-CoV infects human nervous system derived cell lines and primary porcine astrocytes. It is possible that if MERS-CoV gains access to the human CNS, through disruption of the blood brain barrier, via lymphatics [47], or other routes, there are cells expressing DPP4 that could support virus replication. Current knowledge is limited by the absence of any published postmortem data from persons dying from MERS. Interestingly, Arabi and colleagues recently described three MERS patients with severe neurologic manifestations including altered consciousness and diffuse brain abnormalities on MRI involving the white matter and subcortical areas of the frontal, temporal, and parietal lobes, the basal ganglia, and corpus callosum [25]. While there are many reasons that severely ill MERS patients might manifest neurologic signs and symptoms, this report indicates that MERS can be associated with progressive neurological

manifestations. Further data are needed to understand whether some patients with MERS have CNS involvement with infection.

In summary, these MERS mouse models provide a resource for the investigation of early disease mechanisms and therapeutic interventions and provide an economic alternative to other available models of the infection.

Supplementary Materials

Supplementary materials are available at *The Journal of Infectious Diseases* online (http://jid.oxfordjournals.org). Supplementary materials consist of data provided by the author that are published to benefit the reader. The posted materials are not copyedited. The contents of all supplementary data are the sole responsibility of the authors. Questions or messages regarding errors should be addressed to the author.

REFERENCES

1. Zaki AM, van Boheemen S, Bestebroer TM, Osterhaus AD, Fouchier RA. Isolation of a novel coronavirus from a man with pneumonia in Saudi Arabia. N Engl J Med **2012**; 367:1814-20.

2. Raj VS, Mou H, Smits SL, et al. Dipeptidyl peptidase 4 is a functional receptor for the emerging human coronavirus-EMC. Nature **2013**; 495:251-4.

3. Zumla AI, Hui DS, Perlman S. Middle East respiratory syndrome. The Lancet **2015**; DOI 10.1016/S0140-6736(15)60454-8.

4. Saad M, Omrani AS, Baig K, et al. Clinical aspects and outcomes of 70 patients with Middle East respiratory syndrome coronavirus infection: a single-center experience in Saudi Arabia. Int J Infect Dis **2014**; 29:301-6.

5. Arabi YM, Arifi AA, Balkhy HH, et al. Clinical course and outcomes of critically ill patients with Middle East respiratory syndrome coronavirus infection. Ann Intern Med **2014**; 160:389-97.

6. Kapoor M, Pringle K, Kumar A, et al. Clinical and laboratory findings of the first imported case of Middle East respiratory syndrome coronavirus to the United States. Clin Infect Dis **2014**; 59:1511-8.

7. Al-Hameed F, Wahla AS, Siddiqui S, et al. Characteristics and Outcomes of Middle East Respiratory Syndrome Coronavirus Patients Admitted to an Intensive Care Unit in Jeddah, Saudi Arabia. J Intensive Care Med **2015**; DOI 10.1177/0885066615579858.

8. Azhar EI, El-Kafrawy SA, Farraj SA, et al. Evidence for camel-to-human transmission of MERS coronavirus. N Engl J Med **2014**; 370:2499-505.

9. Corman VM, Ithete NL, Richards LR, et al. Rooting the phylogenetic tree of middle East respiratory syndrome coronavirus by characterization of a conspecific virus from an African bat. J Virol **2014**; 88:11297-303.

10. Assiri A, McGeer A, Perl TM, et al. Hospital outbreak of Middle East respiratory syndrome coronavirus. N Engl J Med **2013**; 369:407-16.

11. Hui DS, Perlman S, Zumla A. Spread of MERS to South Korea and China. Lancet Respir Med **2015**; DOI 10.1016/S2213-2600(15)00238-6.

12. Sutton TC, Subbarao K. Development of animal models against emerging coronaviruses: From SARS to MERS coronavirus. Virology **2015**; 479-480C:247-58.

13. Falzarano D, de Wit E, Feldmann F, et al. Infection with MERS-CoV causes lethal pneumonia in the common marmoset. PLoS Pathog **2014**; 10:DOI 10.1371/journal.ppat.1004250.

14. van Doremalen N, Miazgowicz KL, Milne-Price S, et al. Host species restriction of Middle East respiratory syndrome coronavirus through its receptor, dipeptidyl peptidase 4. J Virol **2014**; 88:9220-32.

15. Barlan A, Zhao J, Sarkar MK, et al. Receptor variation and susceptibility to Middle East respiratory syndrome coronavirus infection. J Virol **2014**; 88:4953-61.

16. Zhao J, Li K, Wohlford-Lenane C, et al. Rapid generation of a mouse model for Middle East respiratory syndrome. Proc Natl Acad Sci U S A **2014**; 111:4970-5.

17. Agrawal AS, Garron T, Tao X, et al. Generation of transgenic mouse model of Middle East Respiratory Syndrome-Coronavirus infection and disease. J Virol **2015**; 89:3659-70.

18. Chow YH, Plumb J, Wen Y, et al. Targeting transgene expression to airway epithelia and submucosal glands, prominent sites of human CFTR expression. Mol Ther **2000**; 2:359-67.

19. Chow YH, O'Brodovich H, Plumb J, et al. Development of an epithelium-specific expression cassette with human DNA regulatory elements for transgene expression in lung airways. Proc Natl Acad Sci U S A **1997**; 94:14695-700.

20. McCray PB, Jr., Pewe L, Wohlford-Lenane C, et al. Lethal infection of K18-hACE2 mice infected with severe acute respiratory syndrome coronavirus. J Virol **2007**; 81:813-21.

21. Reznikov LR, Dong Q, Chen JH, et al. CFTR-deficient pigs display peripheral nervous system defects at birth. Proc Natl Acad Sci U S A **2013**; 110:3083-8.

22. Lambeir AM, Durinx C, Scharpe S, De Meester I. Dipeptidyl-peptidase IV from bench to bedside: an update on structural properties, functions, and clinical aspects of the enzyme DPP IV. Crit Rev Clin Lab Sci **2003**; 40:209-94.

23. Chan RW, Chan MC, Agnihothram S, et al. Tropism of and innate immune responses to the novel human betacoronavirus lineage C virus in human ex vivo respiratory organ cultures. J Virol **2013**; 87:6604-14.

24. Glasser SW, Korfhagen TR, Wert SE, et al. Genetic element from human surfactant protein SP-C gene confers bronchiolar-alveolar cell specificity in transgenic mice. Am J Physiol **1991**; 261:L349-L56.

25. Arabi YM, Harthi A, Hussein J, et al. Severe neurologic syndrome associated with Middle East respiratory syndrome corona virus (MERS-CoV). Infection **2015**; DOI 10.1007/s15010-015-0720-y.

26. Barnes K, Kenny AJ, Turner AJ. Localization of aminopeptidase N and dipeptidyl peptidase IV in pig striatum and in neuronal and glial cell cultures. Eur J Neurosci **1994**; 6:531-7.

27. Schnabel R, Bernstein HG, Luppa H, Lojda Z, Barth A. Aminopeptidases in the circumventricular organs of the mouse brain: a histochemical study. Neuroscience **1992**; 47:431-8.

28. Bourne A, Barnes K, Taylor BA, Turner AJ, Kenny AJ. Membrane peptidases in the pig choroid plexus and on other cell surfaces in contact with the cerebrospinal fluid. Biochem J **1989**; 259:69-80.

29. Mitro A, Lojda Z. Histochemistry of proteases in ependyma, choroid plexus and leptomeninges. Histochemistry **1988**; 88:645-6.

30. Mentzel S, Dijkman HB, Van Son JP, Koene RA, Assmann KJ. Organ distribution of aminopeptidase A and dipeptidyl peptidase IV in normal mice. J Histochem Cytochem **1996**; 44:445-61.

31. Busek P, Stremenova J, Sedo A. Dipeptidyl peptidase-IV enzymatic activity bearing molecules in human brain tumors--good or evil? Front Biosci **2008**; 13:2319-26.

32. Busek P, Stremenova J, Krepela E, Sedo A. Modulation of substance P signaling by dipeptidyl peptidase-IV enzymatic activity in human glioma cell lines. Physiol Res **2008**; 57:443-9.

33. Stremenova J, Krepela E, Mares V, et al. Expression and enzymatic activity of dipeptidyl peptidase-IV in human astrocytic tumours are associated with tumour grade. Int J Oncol **2007**; 31:785-92.

34. Selinger C, Tisoncik-Go J, Menachery VD, et al. Cytokine systems approach demonstrates differences in innate and pro-inflammatory host responses between genetically distinct MERS-CoV isolates. BMC Genomics **2014**; 15:1161.

35. Scheuplein VA, Seifried J, Malczyk AH, et al. High secretion of interferons by human plasmacytoid dendritic cells upon recognition of Middle East Respiratory Syndrome Coronavirus. J Virol **2015**; 89:3859-69.

36. Zhou J, Chu H, Li C, et al. Active replication of Middle East respiratory syndrome coronavirus and aberrant induction of inflammatory cytokines and chemokines in human macrophages: implications for pathogenesis. J Infect Dis **2014**; 209:1331-42.

37. Chu H, Zhou J, Wong BH, et al. Productive replication of Middle East respiratory syndrome coronavirus in monocyte-derived dendritic cells modulates innate immune response. Virology **2014**; 454-455:197-205.

38. Coleman CM, Matthews KL, Goicochea L, Frieman MB. Wild-type and innate immune-deficient mice are not susceptible to the Middle East respiratory syndrome coronavirus. J Gen Virol **2014**; 95:408-12.

39. de Wit E, Prescott J, Baseler L, et al. The Middle East respiratory syndrome coronavirus (MERS-CoV) does not replicate in Syrian hamsters. PLoS One **2013**; DOI 10.1371/journal.pone.0069127.

40. Raj VS, Smits SL, Provacia LB, et al. Adenosine deaminase acts as a natural antagonist for dipeptidyl peptidase 4-mediated entry of the Middle East respiratory syndrome coronavirus. J Virol **2014**; 88:1834-8.

41. de Wit E, Rasmussen AL, Falzarano D, et al. Middle East respiratory syndrome coronavirus (MERS-CoV) causes transient lower respiratory tract infection in rhesus macaques. Proc Natl Acad Sci U S A **2013**; 110:16598-603.

42. Munster VJ, de Wit E, Feldmann H. Pneumonia from human coronavirus in a macaque model. N Engl J Med **2013**; 368:1560-2.

43. Haagmans BL, van den Brand JM, Provacia LB, et al. Asymptomatic Middle East respiratory syndrome coronavirus infection in rabbits. J Virol **2015**; 89:6131-5.

44. Adney DR, van Doremalen N, Brown VR, et al. Replication and shedding of MERS-CoV in upper respiratory tract of inoculated dromedary camels. Emerg Infect Dis **2014**; 20:1999-2005.

45. Johnson RF, Via LE, Kumar MR, et al. Intratracheal exposure of common marmosets to MERS-CoV Jordan-n3/2012 or MERS-CoV EMC/2012 isolates does not result in lethal disease. Virology **2015**; 485:422-30.

46. Jewell NA, Cline T, Mertz SE, et al. Lambda interferon is the predominant interferon induced by influenza A virus infection in vivo. J Virol **2010**; 84:11515-22.

47. Louveau A, Smirnov I, Keyes TJ, et al. Structural and functional features of central nervous system lymphatic vessels. Nature **2015**; DOI 10.1038/nature14432.

FIGURE LEGENDS

1. Generation and characterization of K18-*hDPP4* mice. A) The hDPP4 coding sequence was cloned into a plasmid containing the 5' and 3' genomic regions of the human cytokeratin 18 (K18). The K18 5' genomic region consists of a 2.5 kb upstream genomic sequence, promoter, and first intron of the human K18 gene while the K18 3' region consists of exon 6, intron 6, exon 7, and ~300 bp of 3' UTR of the human K18 gene, including the K18 polyA signal. Immediately upstream of the hDPP4 start codon is a translational enhancer (TE) sequence from alfalfa mosaic virus. B) Four K18-*hDPP4* transgenic founder lines were generated and intranasally inoculated with 1 x 10^5 PFU of MERS-CoV. Lung titers of founder mice were determined by plaque assay at 3 days post infection. n= 6-10 mice/line, mean ± S.D. LOD = limit of detection. C) Quantitative measurement of human DPP4 concentrations in tissues of non-transgenic or K18-*hDPP4* founder line 3 by ELISA. n=3, mean ± S.D.

Figure 2. MERS-CoV infection causes lethal disease in K18-*hDPP4* mice. Animals were inoculated intranasally with 1 x 10^5 PFU of MERS-CoV and A) survival, B) weight, and C) temperature monitored daily. Non-transgenic mice, n = 4; K18-*hDPP4* mice, n = 14. D) MERS-CoV titers in indicated tissues at days 2, 4, and 6 post infection, n = 3-4. E) The copy numbers of viral RNA in indicated tissues at days 2 and 4 post infection were analyzed by qRT-PCR targeting regions within open reading frame (ORF)1b, n=4. All results are expressed as mean ± S.D.

Figure 3. A) Lungs from control (CON) or MERS-CoV infected mice. MERS-CoV infection from days 2, 4 and 6 post infection consistently caused multifocal to patchy consolidation in lung with perivascular and peribronchiolar inflammation (arrows). H&E stain, 40x (top panels) and 200x (bottom panels) magnification. B) Airways were generally intact with uncommon scattered sloughed cells (day 6). Note the very rare multinucleate cells (arrow and inset). C) Late in the course of infection (day 6), degenerating cells and cellular debris (arrow and inset) could be seen filling several lymphatics. D) Vascular thrombi (asterisks) were seen in most cases at days 4 and 6 post infection with adjacent congestion and lesser amounts of necrosis and hemorrhage. E) Edema, characterized by eosinophilic fluid material in airspaces (asterisks), was progressively detected in some cases at days 4 and 6. H&E stain, 200x (E) and 400x (F-I) magnification.

Figure 4. Brain disease in MERS-CoV-infected K18-*hDPP4* and uninfected mice. A) Normal brain from an uninfected mouse. B) MERS-CoV caused lymphocytic perivascular cuffing in the infected brain. C) Infected neuron in hippocampus 6 d.p.i. Note the granular degeneration and basophilic cytoplasmic inclusions (arrow and inset). D) Dying cells undergoing degeneration (arrows and inset, 6 d.p.i.) are detected in highly infected regions such as the thalamus or brainstem. E) Meningeal and perivascular cuffing included neutrophilic infiltrates (arrows, 6 d.p.i.). F) Several degenerating cells had small to granular basophilic cytoplasmic inclusions (arrows, 6 d.p.i.) that were stained with anti-MERS-CoV antibody (inset, brown). Note the neuropil rarefaction. H&E stain, 600x magnification. G – I) Outcomes of K18-*hDPP4* mice infected with different intranasal inocula of MERS-CoV. K18-*hDPP4* mice received 1,000, 100, or 10 PFU of MERS-CoV and monitored for G) survival and H) weight, n=5 mice/group. I) Lungs and brains of mice receiving 10 PFU were harvested 10 days after inoculation or when

they lost 20% of body weight. 3 of 7 MERS-CoV treated mice showed high virus titers in the brains. J) MERS-CoV replicates in cells of the nervous system. Human CNS-derived cell lines (U-138 MG, SK-N-SH), primary porcine astrocytes, a murine astrocytoma cell line (DBT), and African green monkey kidney cells (Vero-81) were infected with MERS-CoV at an MOI of 1. Titers from these cells immediately after infection (Day 0) or 2 d.p.i. were determined by plaque assay. Mean ± S.D., n = 3 replicates/condition.

Figure 5. VRP-MERS-S vaccine immunization or passive immunization protects K18-*hDPP4* mice against MERS-CoV infection. A, B) K18-*hDPP4* mice were immunized with 1 x 10^5 infectious units (IU) of VRP-GFP or VRP-MERS-S in the footpad and boosted with the same dose 4 weeks later. Mice were infected with 1 x 10^5 PFU of MERS-CoV two weeks after the boost. C, D) For passive immunization, non-transgenic mice were immunized as described above. Sera were obtained 2 weeks after boosting and transferred into K18-*hDPP4* mice intraperitoneally 1 day before infected with MERS-CoV. Survival and weights were recorded for active immunization (A and B) and passive immunization (C and D); Mean ± S.D., n=5 mice/group. MERS-CoV titers in lung tissue (E) and brain tissue (F) at 2, 4, 6 d.p.i. in mice with or without passive immunization. Mean ± S.D., n = 3 mice/group.

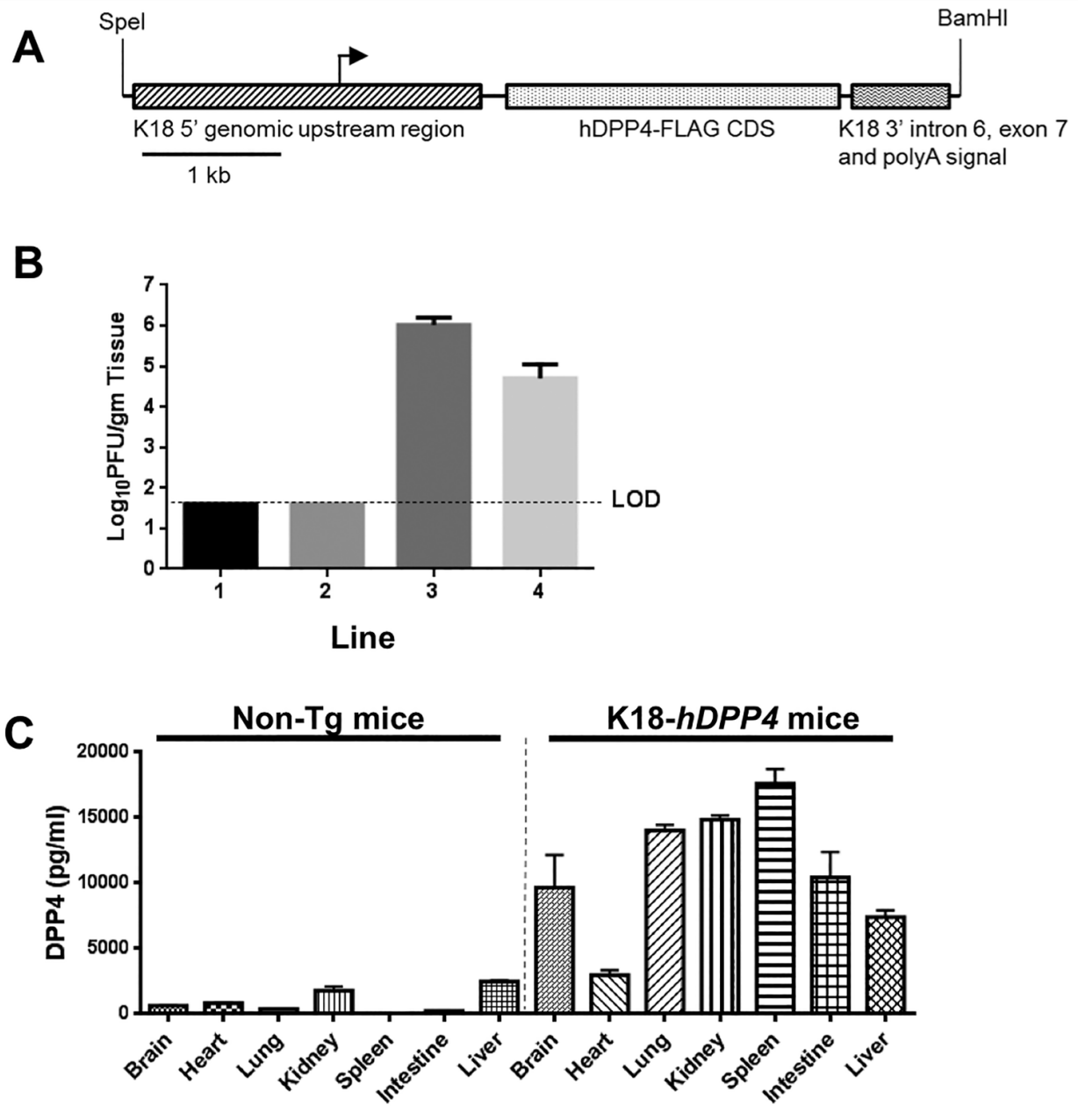
A
SpeI
BamHI
K18 5' genomic upstream region
hDPP4-FLAG CDS
K18 3' intron 6, exon 7 and polyA signal
1 kb
B
Log10PFU/gm Tissue
LOD
Line
C
Non-Tg mice
K18-hDPP4 mice
DPP4 (pg/ml)
Brain
Heart
Lung
Kidney
Spleen
Intestine
Liver

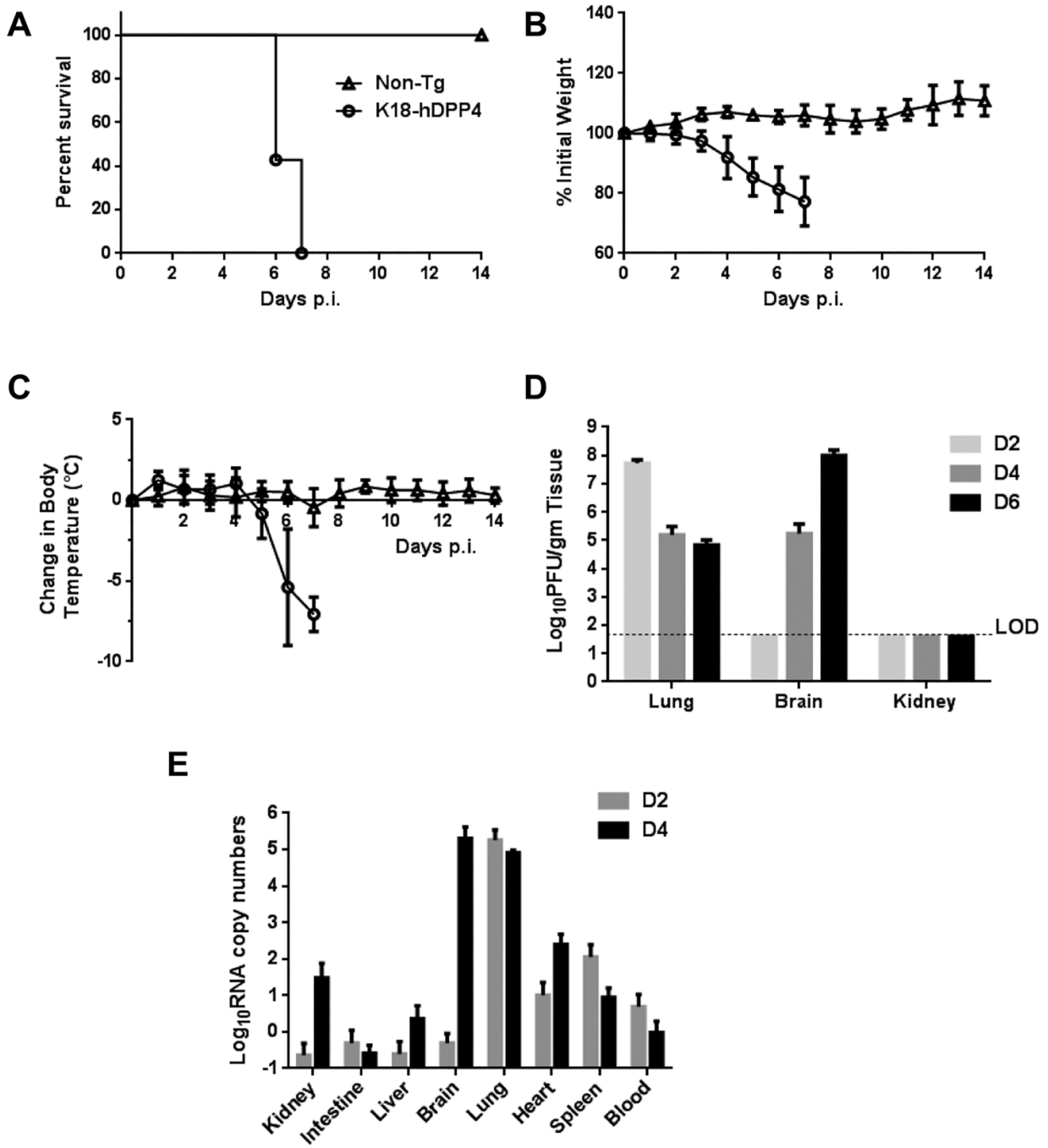
A
Percent survival
Non-Tg
K18-hDPP4
Days p.i.
B
% Initial Weight
Days p.i.
C
Change in Body Temperature (°C)
Days p.i.
D
Log10PFU/gm Tissue
D2
D4
D6
LOD
Lung
Brain
Kidney
E
Log10RNA copy numbers
D2
D4
Kidney
Intestine
Liver
Brain
Lung
Heart
Spleen
Blood

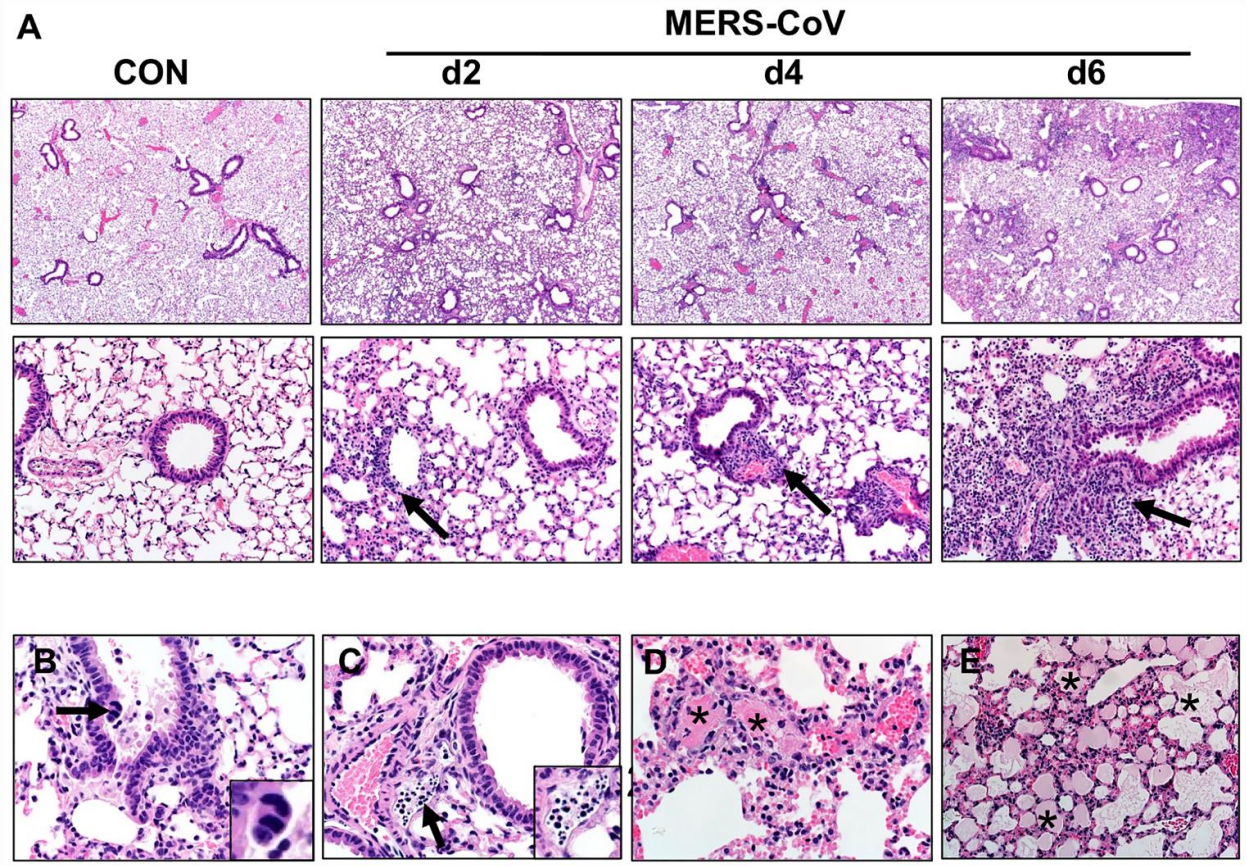

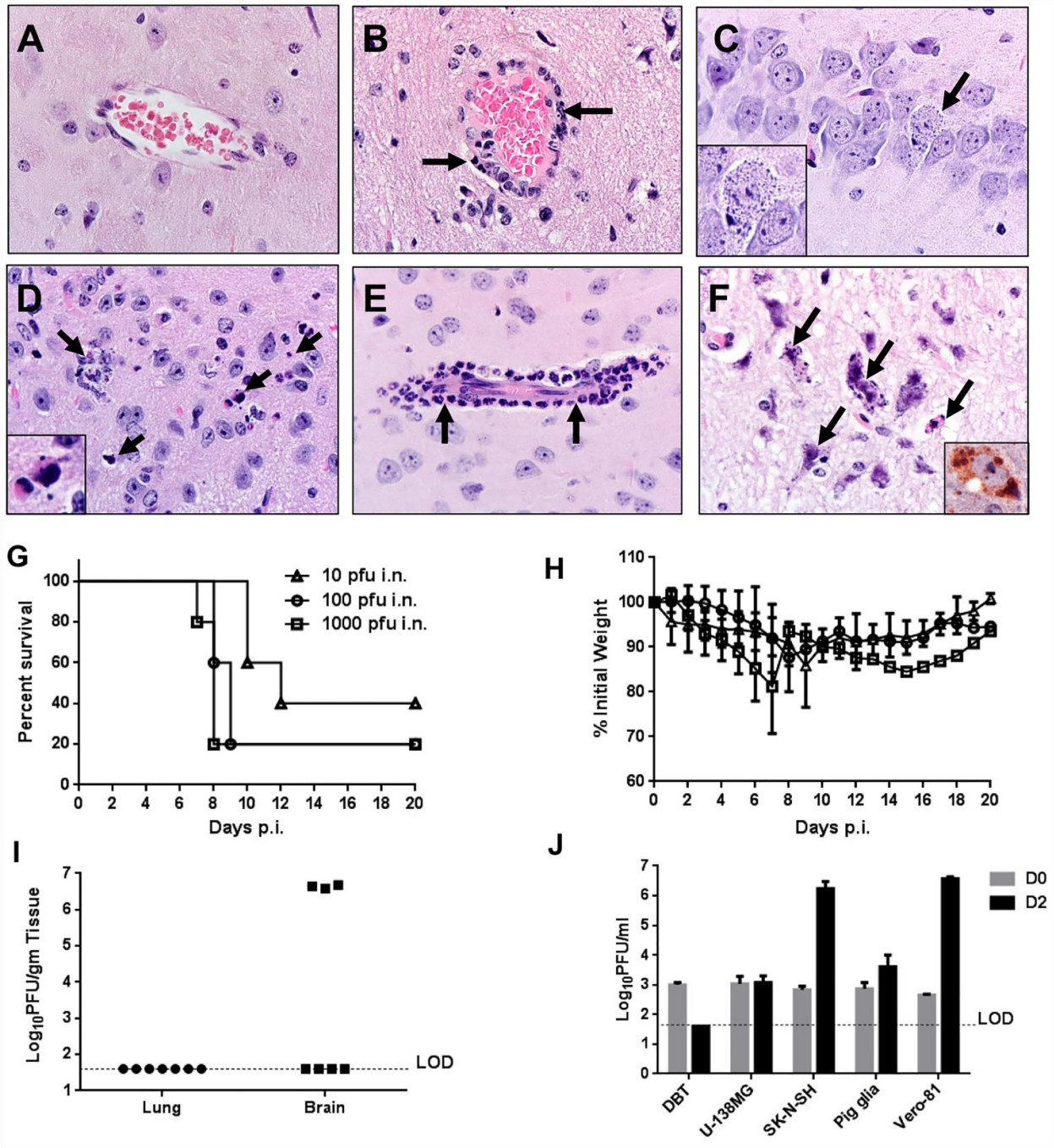
A
B
C
D
E
F
G
Percent survival
10 pfu i.n.
100 pfu i.n.
1000 pfu i.n.
Days p.i.
H
% Initial Weight
Days p.i.
I
Log10PFU/gm Tissue
LOD
Lung
Brain
J
Log10PFU/ml
D0
D2
LOD
DBT
U-138MG
SK-N-SH
Pig glia
Vero-81

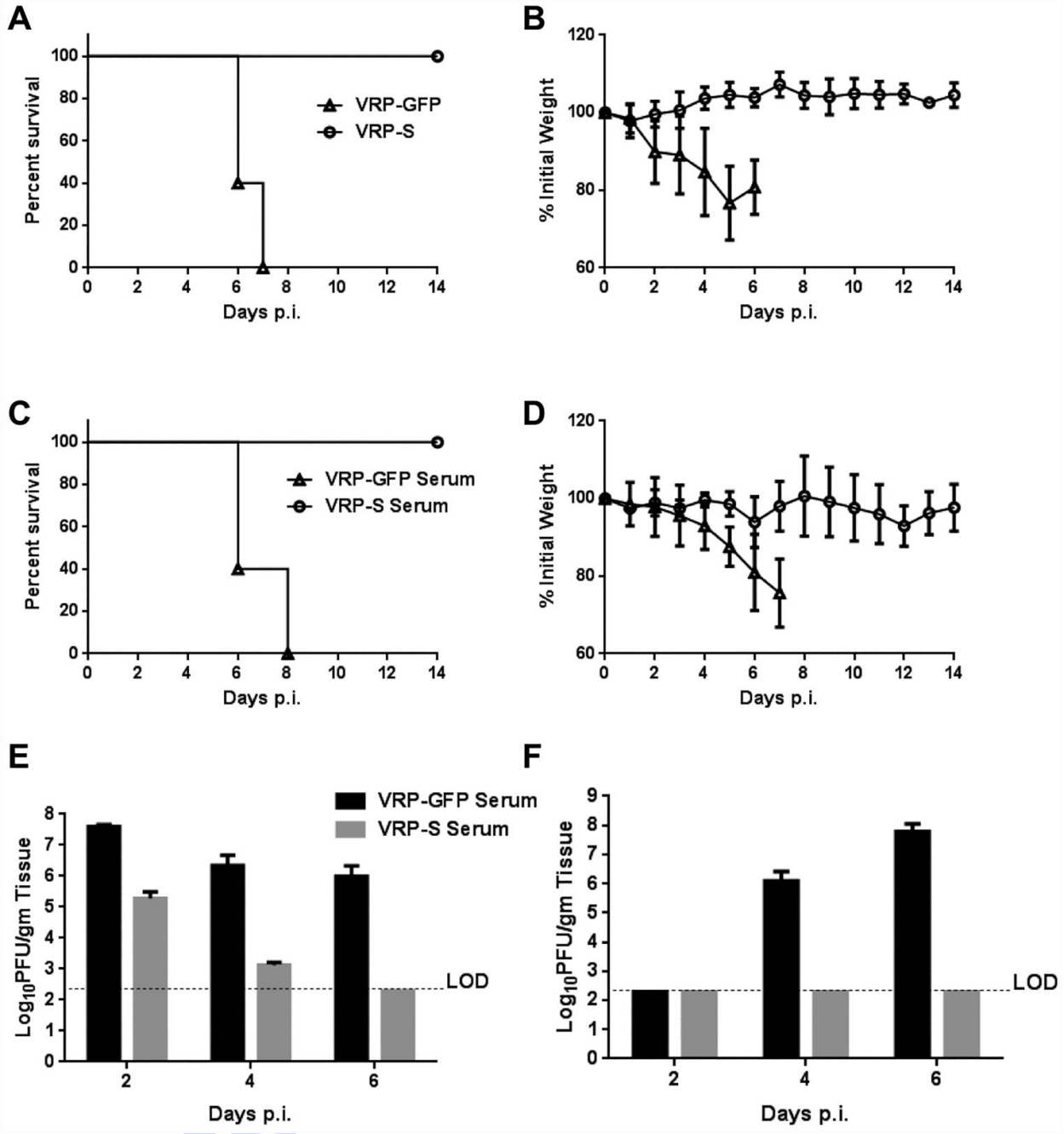
A
Percent survival
VRP-GFP
VRP-S
Days p.i.
B
% Initial Weight
Days p.i.
C
Percent survival
VRP-GFP Serum
VRP-S Serum
Days p.i.
D
% Initial Weight
Days p.i.
E
Log10PFU/gm Tissue
VRP-GFP Serum
VRP-S Serum
LOD
Days p.i.
F
Log10PFU/gm Tissue
LOD
Days p.i.

Table 1. Histopathologic scores (mean +/- SEM) of lung lesions in MERS-CoV infected mice.

	CON n=4	**MERS day 2** n=3	**MERS day 4** n=3	**MERS day 6** n=9
Edema	1 +/- 0.0	1 +/- 0.0 (*P*=0.999)*	1.7 +/- 0.3 (*P*=0.235)	1.6 +/- 0.2 (*P*=0.187)
Consolidation	1.5 +/- 0.3	2.3 +/- 0.3 (*P*=0.999)	3.0 +/- 0.6 (*P*=0.142)	3.3 +/- 0.2 **(*P*=0.004)**
Cell debris lymphatics	1 +/- 0.0	1 +/- 0.0 (*P*=0.999)	1 +/- 0.0 (*P*=0.999)	2.1 +/- 0.2 **(*P*=0.014)**
Thrombi	1 +/- 0.0	1 +/- 0.0 (*P*=0.999)	2.3 +/- 0.3 **(*P*=0.027)**	1.9 +/- 0.2 (*P*=0.058)
Composite score	1.1 +/- 0.1	1.3 +/- 0.1 (*P*=0.999)	2.0 +/- 0.1 (*P*=0.117)	2.2 +/- 0.1 **(*P*=0.002)**

See Methods for scoring parameters. CON = uninfected control

**P*-value represents Dunn's multiple comparison tests versus control (CON day 6)

Table 2. Histopathologic scores (mean +/- SEM) in anatomic regions of brain from MERS-CoV infected mice.

	CON	MERS day 2	MERS day 4	MERS day 6
Brainstem	1 +/- 0.0 (4*)	1 +/- 0.0 (3) (*P*=0.999**)	2.0 +/- 0.0 (2) (*P*=0.696)	4.0 +/- 0.0 (7) **(*P*=0.003)**
Caudate Putamen	1.0 +/- 0.0 (3)	1.0 +/- 0.0 (3) (*P*=0.999)	1.0 +/- 0.0 (3) (*P*=0.999)	2.2 +/- 0.3 (6) (*P*=0.054)
Cerebellum	1 +/- 0.0 (4)	1 +/- 0.0 (2) (*P*=0.999)	1 +/- 0.0 (3) (*P*=0.999)	1.3 +/- 0.3 (4) (*P*=0.607)
Cerebrum	1 +/- 0.0 (4)	1 +/- 0.0 (3) (*P*=0.999)	1.0 +/- 0.0 (3) (*P*=0.999)	1.8 +/- 0.2 (8) **(*P*=0.035)**
Ependyma	1.0 +/- 0.0 (4)	1.0 +/- 0.0 (3) (*P*=0.999)	1.0 +/- 0.0 (3) (*P*=0.999)	1.3 +/- 0.2 (7) (*P*=0.510)
Hippocampus	1.0 +/- 0.0 (2)	1.0 +/- 0.0 (3) (*P*=0.999)	1.0 +/- 0.0 (3) (*P*=0.999)	1.4 +/- 0.2 (9) (P=0.581)
Olfactory bulb	1.0 +/- 0.0 (3)	NA	2.0 +/- 0.0 (1) (*P*=NA)	2.0 +/- 0.0 (2) (*P*=NA)
Thalamus	1.0 +/- 0.0 (4)	1.0 +/- 0.0 (3) (*P*=0.999)	2.3 +/- 0.3 (3) (*P*=0.365)	3.4 +/- 0.2 (7) **(*P*=0.004)**

See Methods for scoring parameters. CON = uninfected control

*N per group

***P*-value represents Dunn's multiple comparison tests versus control (CON day 6).